Inorganic Chemistry

ARTICLE

pubs.acs.org/IC

Synthesis and Anion Sensing of Water-Soluble Metallomacrocycles

Liao-Yuan Yao,[†] Lin Qin,[†] Ting-Zheng Xie,[†] Yi-Zhi Li,[‡] and Shu-Yan Yu*[,†]

[†]Laboratory for Self-Assembly Chemistry, Department of Chemistry, Renmin University of China, Beijing 100872, People's Republic of China

[‡]Department of Chemistry, State Key Laboratory of Coordination Chemistry, Coordination Chemistry Institute, Nanjing University, Nanjing 210093, People's Republic of China

Supporting Information

ABSTRACT: The self-assembly of $(TMEDA)Pd(NO_3)_2$ or $(TMEDA)Pt(NO_3)_2$ (where TMEDA = N^1,N^1,N^2,N^2-tetramethylethane-1,2-diamine) and anthracene- or ferrocene-based diimidazole ligands (L^{1-3}) in aqueous solution affords a series of positively charged $[M_2L_2]^{4+}$ dimetallomacrocycles. Their structures were characterized by ^1H NMR and electrospray ionization mass spectrometry and in the cases of $\{[(TMEDA)Pd]_2L^1{}_2\}(NO_3)_4$ (**1**), $\{[(TMEDA)Pd]_2L^1{}_2\}(PF_6)_4$ (**1a**), and $\{[(TMEDA)Pd]_2L^3{}_2\}(NO_3)_4$ (**4**) by single-crystal X-ray diffraction analysis. Interestingly, the NMR spectra of **1** and **1a** revealed that the difference of their structures, as confirmed by X-ray diffraction analysis, was that a NO_3^- of **1** was encapsulated inside the cavity of the basket-shaped metallomacrocycle by C−H···O hydrogen bonds, while PF_6^- of **1a** was bound outside by C−H···F hydrogen bonds. The fluorescence titration experiment exhibited the formation of 1:1 host−guest complexation for anthracene-based positively charged $[M_2L_2]^{4+}$-type metallomacrocycles with NO_3^-. The interactions between metallomacrocycles and various anions were investigated via fluorescence titration and cyclic voltammetry studies, respectively.

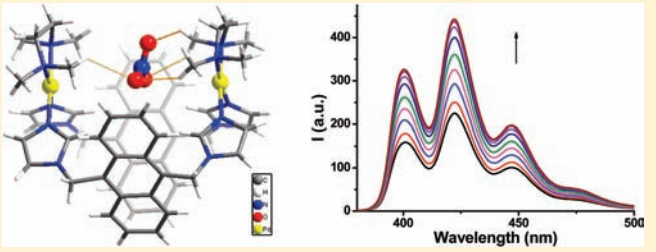

INTRODUCTION

Supramolecular chemistry of anions, pioneered by Lehn in the late 1970s,[1,2] has attracted considerable research attention[2−8] because of the important roles of anions in biology, chemistry, medicine, catalysis, and the environment. Until now, great efforts have been made in the design and synthesis of the receptors for anionic species, most of which have been synthesized through covalent organic synthesis.[3,6a,9] As we know, anions are ubiquitous in biological systems in the form of their aqueous solution, and it represents a challenge to design and synthesize water-soluble receptors for anions. With the rapid development of coordination-driven self-assembly over the past 2 decades,[10] chemists have become interested in the design of self-assembled water-soluble metallomacrocycles with functional ligands for potential uses in anion recognition and sensing. Although metal−organic anion receptors made of molecular metal complexes have been reported recently,[11] self-assembled positively charged water-soluble metallomacrocycles utilized to sense anions in aqueous solution are very rare.

Since 2003, we have developed a series of positively charged water-soluble metallomacrocycles through a cavity-tunable self-assembly approach, such as molecular bowls, crowns, baskets, hats, and clips, which show promise toward the complexation of inorganic anions.[12] Herein, we employed flexible diimidazole ligands with luminescent or redox-active spacers such as anthracene or ferrocene as linkers and metal complexes $(TMEDA)Pd(NO_3)_2$ or $(TMEDA)Pt(NO_3)_2$ as constructing units to synthesize and characterize a series of water-soluble metallomacrocyclic complexes via self-assembly (as shown in Scheme 1). Their anion-sensing properties in aqueous solution were investigated via fluorescence titration for anthracene-based metallomacrocycles and cyclic voltammetry (CV) titration for ferrocene-based metallomacrocycles.

RESULT AND DISSCUSION

Synthesis and Structures of the $[M_2L_2]^{4+}$-Type Metallomacrocycles with Ligands L^1 and L^2. As shown in Scheme 1, $(TMEDA)Pd(NO_3)_2$ or $(TMEDA)Pt(NO_3)_2$ was treated with a suspension containing 1 equiv of L^1 or L^2 (as shown in Scheme 1) in H_2O at room temperature or 60 °C over 12 h. Then the mixture was filtered, and the resulting clear solution was concentrated, leading to the formation of positively charged metallomacrocycles $[M_2L_2](NO_3)_4$ [M = Pd^{II}, L = L^1, **1**; M = Pt^{II}, L = L^1, **2**; M = Pd^{II}, L = L^2, **3**]. The ^1H NMR analysis indicated the formation of a single product. The assignments of $[M_2L_2]^{4+}$-type macrocycles were based on electrospray ionization mass spectrometry (ESI-MS) studies, where multiply charged molecular ions corresponding to intact cyclic dimers were observed. Single-crystal X-ray structural studies of **1** and **1a**

Received: January 11, 2011
Published: June 09, 2011

Scheme 1. Synthesis of $[M_2L_2]^{4+}$-Type Metallomacrocycles

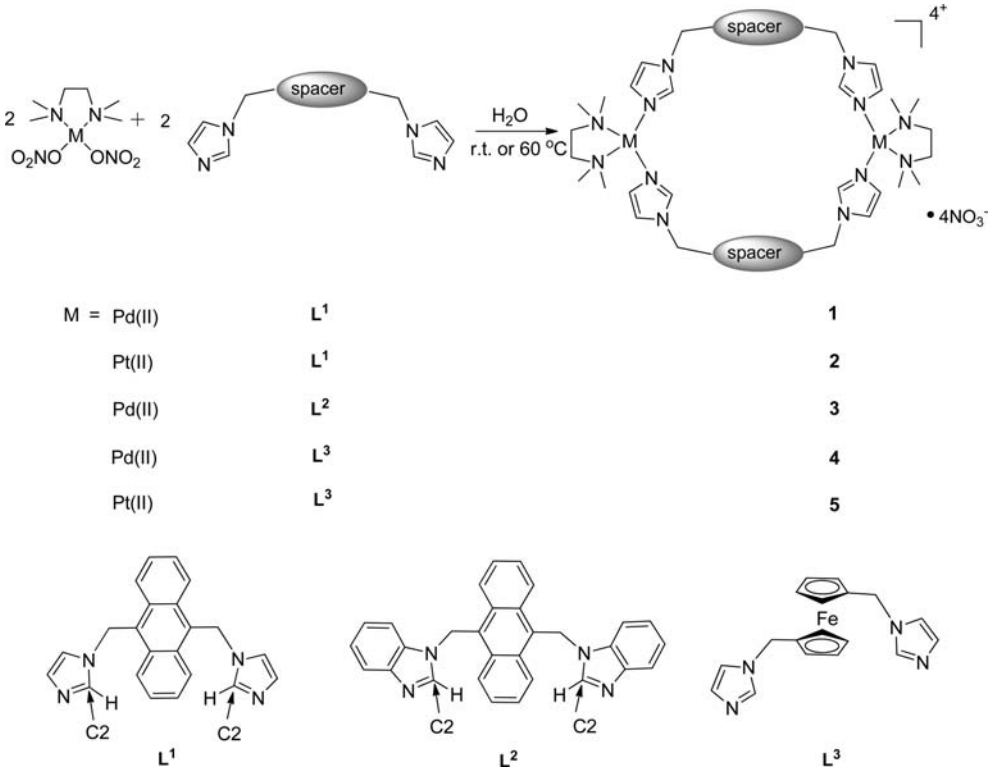

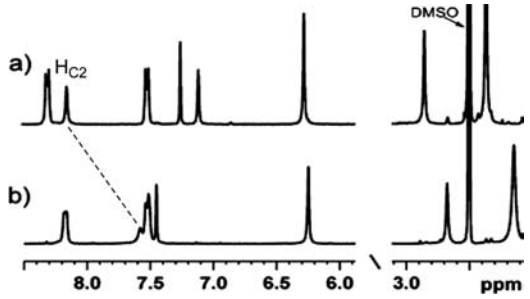

Figure 1. ^{1}H NMR spectra of (a) **1a** and (b) **1** in DMSO-d_6, 25 °C, $Si(CH_3)_4$ (left, peaks of L^1; right, peaks of TMEDA).

(the PF_6^- salt of **1**) confirmed the formation of $[M_2L_2]^{4+}$-type macrocycles.

The ^{1}H NMR spectra of **1** and **1a** in Figure 1 clearly showed that 1:1 (TMEDA)Pd to diimidazole ligand complexes were formed. It can be seen that several peak shifts were observed when the ^{1}H NMR spectrum of **1a** was compared with that of **1**. The proton signals clearly revealed that $[M_2L_2]^{4+}$ of **1a** was highly symmetric. In contrast, when only the counteranions were changed, some signals of **1** were overlapped and the spectral shape indicated the low symmetry of the metallomacrocycle. In particular, the signal of the proton of C2 in L^1 showed upfield shifts ($\Delta\delta \approx 0.6$ ppm) from **1a** to **1**, which indicated the remarkable shielding effect. We deduced that the counteranions PF_6^- of **1a** were located outside of the positively charged macrocycle, while the NO_3^- anions of **1** were encapsulated inside the macrocycle through hydrogen bonds, which was confirmed by the single-crystal X-ray diffraction analyses of **1** and **1a**.

The ^{1}H NMR spectrum of **2** showed behavior similar to that of **1** (Figure S3 in the Supporting Information). Owing to the steric effects of benzimidazole in L^2 (as shown in Scheme 1), the geometry of complex **3** resulted in two different environments for all groups caused by the fixed structure (as shown in Figure 2). As a result, two sets of metallomacrocycles, except the proton of C2 in L^2, were observed by ^{1}H NMR (Figure S4 in the Supporting Information).

The formation of the $[M_2L_2]^{4+}$-type metallomacrocyclic structure was further supported by ESI-MS in methanol. ESI-MS spectra of **1**−**3** in a methanol solution allowed the unambiguous assignment of $[(TMEDA)Pd]_2L^1{}_2$, $[(TMEDA)Pt]_2L^1{}_2$, and $[(TMEDA)Pd]_2L^2{}_2$. As shown in Figure 3, the multiply charged molecular ions of **1** were observed at m/z 1308.4 ($[\mathbf{1}-NO_3^-]^+$), 623.2 ($[\mathbf{1}-2NO_3^-]^{2+}$), 394.5 ($[\mathbf{1}-3NO_3^-]^{3+}$), and 280.6 ($[\mathbf{1}-4NO_3^-]^{4+}$). Similarly, the multiply charged molecular ions of **2** were at m/z 711.7 ($[\mathbf{2}-2NO_3^-]^{2+}$), 324.8 ($[\mathbf{2}-4NO_3^-]^{4+}$) (Figure S5 in the Supporting Information), and the multiply charged molecular ions of **3** were at m/z 1508.4 ($[\mathbf{3}-NO_3^-]^+$), 723.2 ($[\mathbf{3}-2NO_3^-]^{2+}$), 461.5 ($[\mathbf{3}-3NO_3^-]^{3+}$), 330.6 ($[\mathbf{3}-4NO_3^-]^{4+}$) (Figure S6 in the Supporting Information), respectively.

The ORTEP diagram of **1** is shown in Figure 4. Complex **1** crystallizes in the monoclinic space group $P2(1)/c$. The crystal structure analysis for **1** reveals the Pd_2 basket-shaped macrocyclic structure with two (TMEDA)Pd units. The two anthracene rings form a dihedral angle of 60°. The dihedral angles between the two imidazole (N3−N4 and N5−N6; N9−N10 and N11−N12) planes at each corner are 86.8 and 85.7°, respectively, which are a little smaller than the angles of N2−Pd1−N3 and N7−Pd2−N9 [92.35(16) and 90.68(14)°]. The distance of Pd1−Pd2 is 8.02 Å. The cavity of the Pd_2 basket-shaped macrocycle with several protons inside can encapsulate guest molecules and anions. In

dx.doi.org/10.1021/ic200047t |*Inorg. Chem.* 2011, 50, 6055–6062

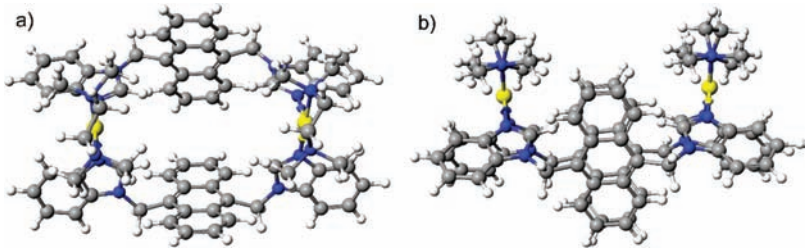

Figure 2. Optimized geometry of **3** (ball-and-stick model calculated with the *CAChe 6.1.1* program): (a) top view; (b) side view (yellow, Pd; gray, C; white, H; blue, N).

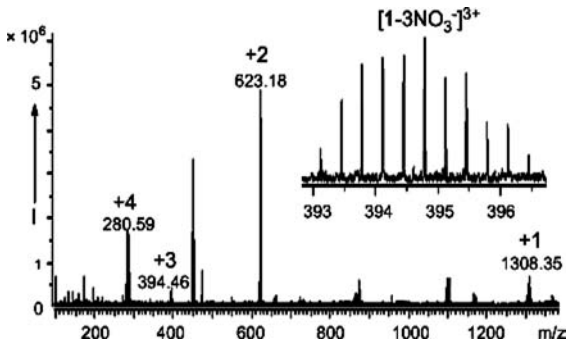

Figure 3. ESI-MS spectrum of **1** in methanol. The inset shows the isotopic distribution of the species $[\mathbf{1}-3NO_3^-]^{3+}$.

this case, as shown in Figure 4, one NO_3^- is encapsulated in the cavity through hydrogen bonds between the C−H and O atoms. The selected lengths and angles of the hydrogen bonds are as follows: C4−H4A···O2, 2.40 Å, 138°; C4−H4B···O3, 2.55 Å, 121°; C6−H6C···O1, 2.35 Å, 144°; C9−H9A···O1, 2.59 Å, 122°.

The ORTEP diagram of **1a** is shown in Figure 5. Complex **1a** crystallizes in the monoclinic space group *C*2/*c*. Crystal structure analysis for **1a** reveals the Pd_2 square-shaped macrocyclic structure with two (TMEDA)Pd constructing units. The two anthracene planes are parallel, separated by approximately 7 Å. The dihedral angle between the two imidazole (N3−N4 and N5−N6) planes at each corner is 74.1°. The angle of N3−Pd1−N5 is 87.05(15)°, which is a little smaller than the angles of N2−Pd1−N3 and N1−Pd1−N5 [94.86(15) and 92.30(17)°]. The distance of Pd1−Pd1A is 12.90 Å. The cavity of the Pd_2 square-shaped macrocycle shows promise in encapsulating guest molecules and anions. As shown in Figure 5, one PF_6^- is bonded through hydrogen bonds between C−H and F atoms. The selected lengths and angles of the hydrogen bonds are, for example, as follows: C7−H7···F1, 2.38 Å, 167°; C7−H7···F3, 2.51 Å, 132°. These hydrogen-bond C−H···F distances were smaller than that previously found between CH and fluoride (2.58 Å).[9b]

Synthesis and Structures of the $[M_2L_2]^{4+}$-Type Metallomacrocycles with Ligand L^3. As shown in Scheme 1, simply mixing (TMEDA)Pd$(NO_3)_2$ or (TMEDA)Pt$(NO_3)_2$ with a suspension containing 1 equiv of L^3 in H_2O at room temperature or 60 °C over 12 h resulted in positively charged metallomacrocycles $[M_2L_2](NO_3)_4$ [M = Pd^{II}, **4**; M = Pt^{II}, **5**]. The ^{1}H NMR spectra of **4**, **4a** (the PF_6^- salt of **4**), and **5** clearly showed that a 1:1 mixture of (TMEDA)Pd or (TMEDA)Pt to the ferrocene-based diimidazole ligand complexes was formed (Figures S7−S9 in the Supporting Information).

The assignments of $[M_2L_2]^{4+}$-type metallomacrocycles were based on ESI-MS studies, where multiply charged molecular ions corresponding to intact cyclic dimers were observed. ESI-MS spectra of **4** and **5** in a methanol solution allowed the unambiguous assignment of $[(TMEDA)Pd]_2L^3{}_2$ and $[(TMEDA)Pt]_2L^3{}_2$ products, respectively. The multiply charged molecular ions of **4** were at *m*/*z* 630.6 ($[\mathbf{4}-2NO_3^-]^{2+}$), 399.7 ($[\mathbf{4}-3NO_3^-]^{3+}$), 284.4 ($[\mathbf{4}-4NO_3^-]^{4+}$) (Figure S10 in the Supporting Information). Similarly, the multiply charged molecular ions of **5** were observed at *m*/*z* 1501.3 ($[\mathbf{5}-NO_3^-]^+$), 719.7 ($[\mathbf{5}-2NO_3^-]^{2+}$), 459.1 ($[\mathbf{5}-3NO_3^-]^{3+}$), and 328.8 ($[\mathbf{5}-4NO_3^-]^{4+}$) (Figure S11 in the Supporting Information). Eventually, formation of the $[M_2L_2]^{4+}$-type metallomacrocycle was confirmed by a single-crystal X-ray structural study of **4** (Figure 6).

The ORTEP diagram of **4** is shown in Figure 6. Complex **4** crystallizes in the triclinic space group $P\bar{1}$. Crystal structure analysis for **4** reveals the Pd_2 square-shaped macrocyclic structure with two (TMEDA)Pd constructing units. The four cyclopentadiene rings of ferrocenes are parallel to each other. The dihedral angle between the two imidazole (N3−N4 and N2−N1) planes at each corner is 78.9°. The angle of N1−Pd1−N3 is 87.61(16)°, which is a little smaller than the angles of N1−Pd1−N6 and N3−Pd1−N5 [93.35(17) and 93.31(16)°]. The distance of Pd1−Pd1A is 12.70 Å. The cavity of the Pd_2 square-shaped macrocycle is small because of the $\pi-\pi$ stacking of the cyclopentadiene rings of ferrocene. As shown in Figure 6, one NO_3^- is bonded through the hydrogen bonds between C−H and O atoms. The selected lengths and angles of the hydrogen bonds are, for example, as follows: C16−H16···O4, 2.43 Å, 166°; C16−H16···O6, 2.54 Å, 146°.

The UV−vis absorption spectra of metallomacrocycles **4** and **4a** showed absorption bands at 429−433 nm in dilute methanol and in dilute acetonitrile, respectively. The absorption bands typical of iron bis(cyclopentadienyl) are independent of the substituents on the ferrocene ring as well as of the anions[13] (Figure S12 in the Supporting Information).

Anion-Sensing Properties. *Anion Sensing for Luminescent Metallomacrocycles.* The synthesis of **1** has been achieved through self-assembly in aqueous solution (Scheme 1). In water, **1** exhibits a characteristic anthracene emission and fluorescence maxima at 401, 422, and 447 nm (excitation at 370 nm) and UV−vis spectrum peaks at 339, 356, 374, and 395 nm, respectively (Figure S13 in the Supporting Information). The PF_6^- salt of **1** (**1a**) was obtained by exchange with excess NH_4PF_6 in a methanol solution in quantitative yield. More interestingly, from the NMR analysis experiments of **1a** and **1** in DMSO-d_6, several peak shifts were observed when the ^{1}H NMR spectrum of **1a** was compared with that of **1** (as shown in Figure 1). This NMR feature establishes that the geometries of **1a** and **1** are different in

dx.doi.org/10.1021/ic200047t |*Inorg. Chem.* 2011, 50, 6055–6062

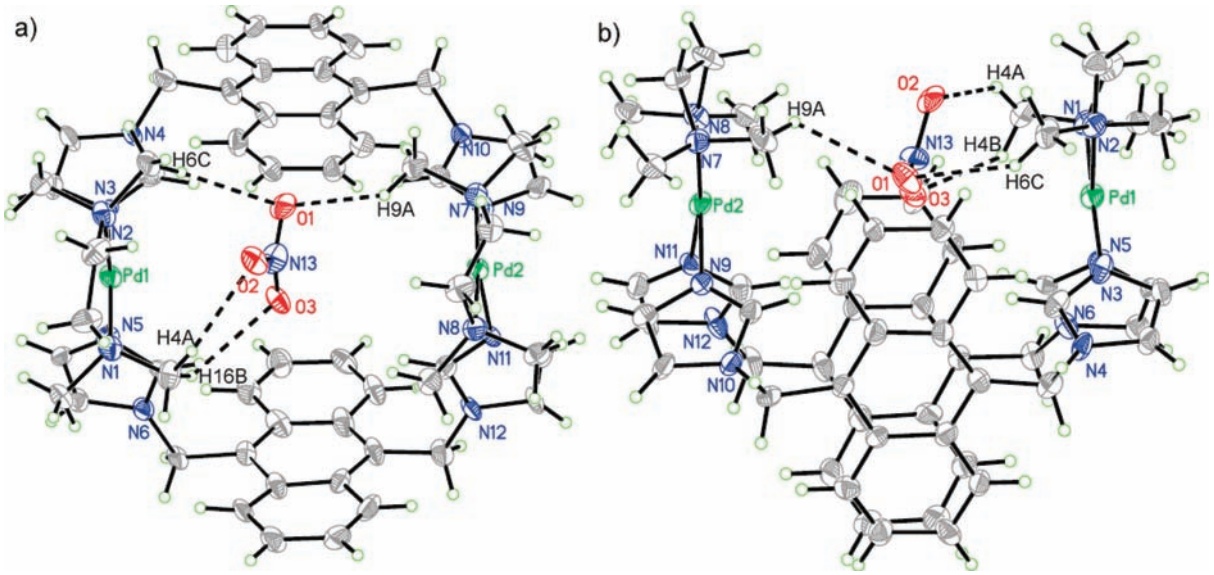

Figure 4. ORTEP diagram of the molecular structure of **1**: (a) top view; (b) side view. Thermal ellipsoids are shown at the 30% probability level. The remaining counteranions and solvent molecules are omitted for clarity.

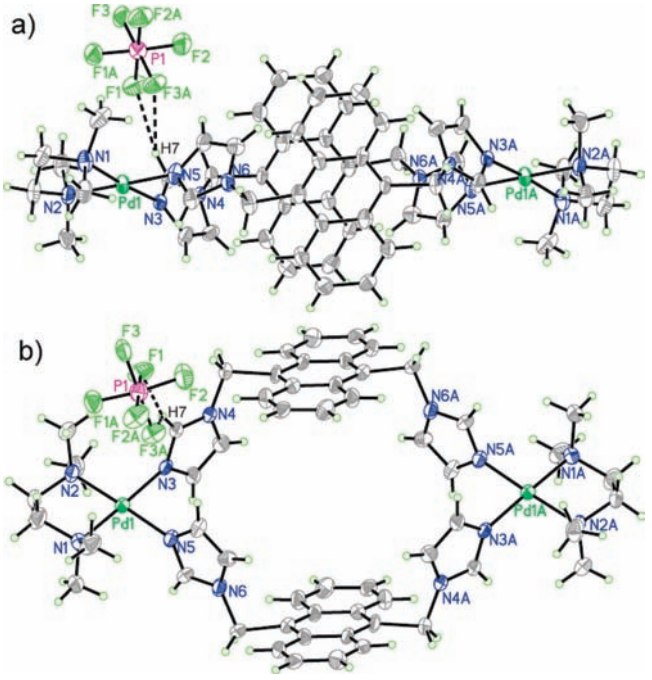

Figure 5. ORTEP diagram of the molecular structure of **1a**: (a) side view; (b) top view. Thermal ellipsoids are shown at the 30% probability level. The remaining counteranions and solvent molecules are omitted for clarity.

the solution state, as revealed by the X-ray structure analysis of **1** and **1a** in the solid state, which indicates that NO_3^- of **1** was encapsulated inside the cavity of the basket-shaped metallomacrocycle by C−H···O hydrogen bonds, while PF_6^- of **1a** was bonded outside by C−H···F hydrogen bonds.

On the basis of the NMR and X-ray structure analysis, to further investigate the mechanism of encapsulation of NO_3^- for positively charged metallomacrocycle, fluorescence titration experiments were carried out. The addition of aliquots of NO_3^- to a solution of **1a** in H_2O/CH_3CN (2:1, v/v; 1.0×10^{-5} M) resulted in a linear increase of the fluorescence intensity until it reached 1 equiv concentration (1.0×10^{-5} M). The fluorescence titration curve of NO_3^- suggested the formation of a 1:1 complex between positively charged metallomacrocyle and NO_3^- (Figure 7). Also, Job's plot showed that the stoichiometry of the receptor **1a** with NO_3^- was 1:1 (Figure S14 in the Supporting Information). In the concentration range 2.0×10^{-6}—1.0×10^{-5} M, there is a good linear relationship between the concentration and fluorescence intensity, which indicates that the limit of detection on NO_3^- based on **1a** can reach 2.0×10^{-6} M.

For the fluorescence quantum yield (Φ_f) determination, the quinine sulfate was chosen as a standard (Φ_f = 0.55) and the quantum yields of **1a** and the 1:1 complex (**1a**·NO_3^-) were reported as 0.040 and 0.079, respectively. It can be seen that the value of Φ_f of **1a** upon the addition of 1 equiv of NO_3^- is 2-fold that of free **1a**.[14] Obvious fluorescence emission enhancements were also observed upon the addition of F^- to the solution of **1a** in H_2O/CH_3CN (2:1, v/v; 1.0×10^{-5} M; Figure S15 in the Supporting Information). However, we could not obtain reliable association constants for these two anions from the fluorescent experiment because the reversibility of the complexation processes could not be proven and the emission intensity did not consistently increase upon the addition of F^-. Upon sensing, no remarkable anion binding that induced changes in the absorption spectra could be detected.

The anion-sensing properties of the luminescent water-soluble metallomacrocycle **1** were investigated through fluorescence titration in aqueous solution. Fluorescence changes of **1** in H_2O (1.0×10^{-5} M) upon the addition of anions (SO_4^{2-}, NO_3^-, HSO_4^-, F^-, and $H_2PO_4^-$) were investigated (Figure S16 in the Supporting Information). The strong fluorescence enhancement induced by HSO_4^- allowed it to be discriminated from the other anions. However, for the reason that only a slight fluorescence enhancement was observed upon the addition of SO_4^{2-}, it was very possible that just H^+ dissociated from HSO_4^- had caused the enhancement, which was confirmed by the remarkable fluorescence enhancement observed upon the addition of HNO_3 (100 equiv) because nitrate itself had a slight effect

dx.doi.org/10.1021/ic200047t |*Inorg. Chem.* 2011, 50, 6055–6062

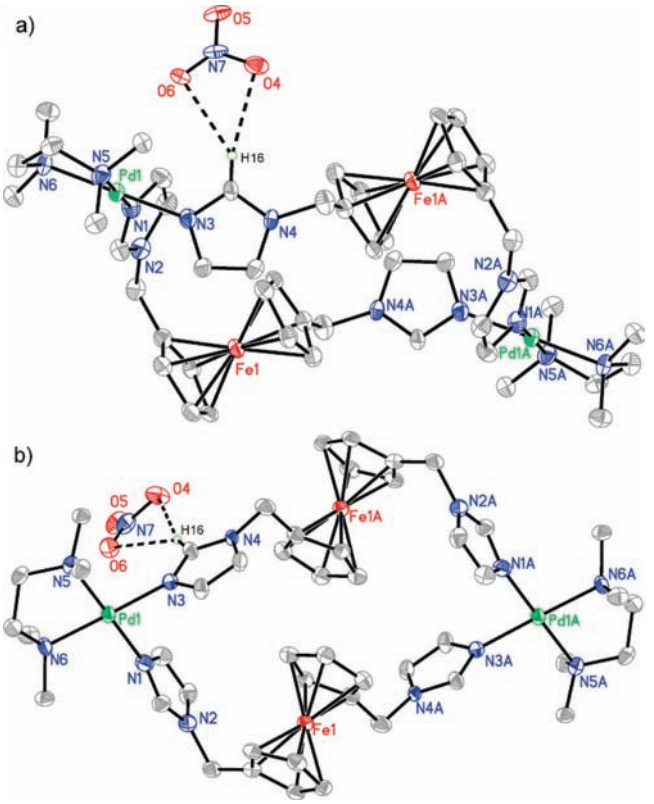

Figure 6. ORTEP diagram of the molecular structure of **4**: (a) side view; (b) top view. Thermal ellipsoids are shown at the 30% probability level. The remaining counteranions, H atoms (except H16), and solvent molecules are omitted for clarity.

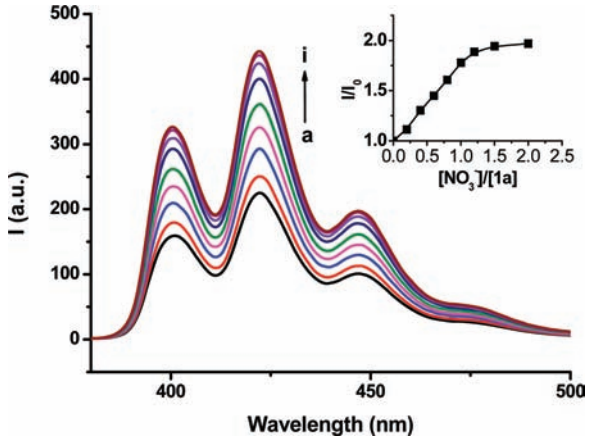

Figure 7. Fluorescent emission of **1a** in H_2O/CH_3CN (2:1, v/v; 1.0×10^{-5} M) upon the addition of NO_3^-: (a) 0, (b) 0.2, (c) 0.4, (d) 0.6, (e) 0.8, (f) 1.0, (g) 1.2, (h) 1.5, and (i) 2.0 equiv. The inset shows the emission titration curve of **1a** upon the addition of NO_3^- at 422 nm. λ_{ex} = 370 nm.

(Figure S16 in the Supporting Information). To gain more insight into the sensing mechanism, fluorescence titration of HSO_4^- (Figure S17 in the Supporting Information) and other anions were carried out but were confusing. Therefore, it was not possible to obtain accurate association constants for these anions.

The fluorescence is switched on upon sensing rather than switched off as was reported in many literature cases.[6b] One possible mechanism is that the addition of anions may inhibit the quenching of excited states involving either energy or electron transfer caused by metal−organic complexes, so as to allow fluorescence of the receptors to be restored.[15]

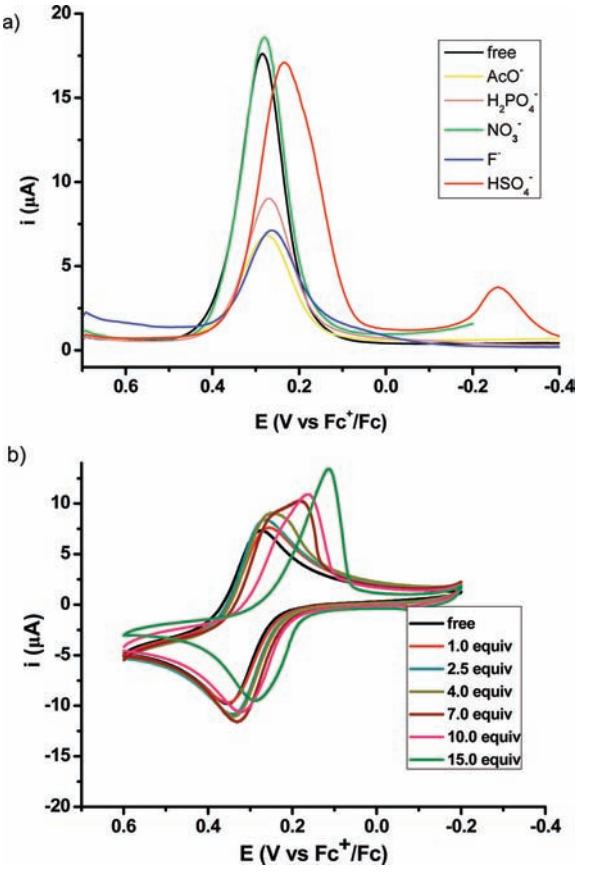

Figure 8. (a) Evolution of the SWV of receptor **4a** in CH_3CN upon the addition of various anions (4 equiv). (b) CV of receptor **4a** in CH_3CN upon the addition of various concentrations of HSO_4^-. Supporting electrolyte: 0.1 M $(n\text{-Bu})_4NPF_6$. Scan rate: 100 mV/s.

Anion Sensing for Redox-Active Metallomacrocycles. For the redox-active group ferrocene employed in the formation of metallomacrocycles, CV experiments of **4** and **4a** (the PF_6^- salt of **4**) were carried out. Each macrocycle exhibited a reversible one-electron redox wave (Figure S18 in the Supporting Information), typical of ferrocene derivatives. Compared to unsubstituted ferrocene, $E_{1/2}$'s for **4** and **4a** shifted to more positive potentials (220−229 mV vs Fc^+/Fc) because of the electron-withdrawing effect of the imidazolium groups and of the metals.

The anion-sensing properties of receptor **4a** (5.0×10^{-4} M) were investigated by CV and square-wave voltammetry (SWV) in CH_3CN solutions containing 0.1 M $(n\text{-Bu})_4NPF_6$ as the supporting electrolyte. The electrochemical behaviors of the receptor alone and in the presence of various concentrations of anions (HSO_4^-, F^-, $H_2PO_4^-$, AcO^-, and NO_3^-) were studied.

In order to make a good estimation about the $E_{1/2}$ values, SWV was employed to obtain well-resolved potential information. As seen from Figure 8a, the addition of different anions to the CH_3CN solution of **4a** caused different behaviors on SWV. The resulting ΔE_p values versus the free receptor are reported in Table 1. The presence of NO_3^- had few changes on SWV, while the addition of $H_2PO_4^-$, AcO^-, and F^- led to a decrease in the

dx.doi.org/10.1021/ic200047t |*Inorg. Chem.* 2011, 50, 6055–6062

Table 1. E_p and ΔE_p Values Associated with the Complexing Processes between the Free Receptor and the Appropriate Anion

	anion					
	free	HSO_4^-	F^-	$H_2PO_4^-$	AcO^-	NO_3^-
E_p (mV)	284	232	264	268	272	280
ΔE_p (mV vs free)	0	−52	−20	−16	−12	−4

current. Compared to the other anions, the addition of HSO_4^- caused the most obvious changes of the E_p values and had the strongest interaction with the redox center. Furthermore, when HSO_4^- was added, a second wave at more negative potential appeared, which could be attributed to the formation of a receptor−anion complex.[16]

The CV titrations of these anions were carried out in a 0.1 M $(n\text{-Bu})_4NPF_6$−CH_3CN solution (Figures 8b and S19−S21 in the Supporting Information). The addition of HSO_4^- to the CH_3CN solution of receptor **4a**, unlike the other anions, exhibited some different behaviors on CV. From Figure 8b, it can be seen that, after the concentration of HSO_4^- reached 4 equiv, another cathodic peak appeared and its current increased. Finally, the original cathodic peak disappeared and was replaced by another cathodic peak with higher current. These behaviors on CV could be attributed to the formation of a receptor−anion complex, which has been demonstrated by the SWV experiment before. The addition of HSO_4^- to the CH_3CN solution of receptor **4a** induced the cathodic peak current to increase, which may be attributed to hydrogenation at the iron center, which consumes the receptors in a reduction reaction.[17]

CONCLUSIONS

Luminescent or redox-active diimidazolate-bridged metallomacrocycles with palladium(II) or platinum(II) centers can be obtained from $(TMEDA)Pd(NO_3)_2$ or $(TMEDA)Pt(NO_3)_2$ and diimidazole ligands in a 1:1 molar ratio in water. The structures of metallomacrocyclic assemblies $\{[(TMEDA)Pd]_2L^1_2\}^{4+}$ have been transformed by alteration of the counteranions from NO_3^- (**1**) to PF_6^- (**1a**), as revealed by ^1H NMR analysis in the solution state and X-ray structure analysis in the solid state. The fluorescence titration experiment indicated that the 1:1 host−guest complexation of metallomacrocyclic assemblies $\{[(TMEDA)Pd]_2L^1_2\}^{4+}$ with NO_3^- was formed. In addition, the anion sensing for metallomacrocycles was investigated via fluorescence and CV titration. These positively charged water-soluble metallomacrocycles are capable of being utilized in anion recognition and sensing in aqueous solution.

EXPERIMENTAL SECTION

Materials. All chemicals and solvents were of reagent grade and were purified according to conventional methods.[18] The metal−organic complexes $(TMEDA)Pd(NO_3)_2$ and $(TMEDA)Pt(NO_3)_2$ (where TMEDA = N^1,N^1,N^2,N^2-tetramethylethane-1,2-diamine) were prepared according to literature procedures.[19] The organic ligands 9,10-bis(imidazol-1-ylmethyl)-anthracene (L^1), 9,10-bis(benzimidazol-1-ylthmethyl)anthracene (L^2), and 1,1′-bis(imidazolylmethyl)ferrocene (L^3) were synthesized according to published methods.[20−22]

Instrumentation. ^1H NMR experiments were performed on a Bruker Avance DMX400 spectrometer using tetramethylsilane $[Si(CH_3)_4]$ as an internal standard. ESI-MS measurements were performed with an HP5989B mass spectrometer.

Elemental analyses were performed on a Thermoquest Flash EA 1112 instrument. UV−visible absorption spectra were obtained on a Cary 50 Probe UV−visible spectrophotometer. Fluorescence spectra were measured using a PerkinElmer instruments luminescence spectrophotometer. Fluorescent titrations were carried out by the addition of aliquots of various anions as their K^+ salts to receptor **1** (1.0×10^{-5} M) in H_2O and to receptor **1a** (1.0×10^{-5} M) in H_2O/CH_3CN (2:1, v/v), respectively, at 25 °C. Excitation was at 370 nm. Excitation and emission slit widths were 3 and 7 nm, respectively.

CV and SWV studies were performed on a CHI620b electrochemical analyzer in a 0.1 M $(n\text{-Bu})_4NPF_6$−CH_3CN solution with a platinum electrode as the working electrode at 25 °C (scan rate: 100 mV/s). A 0.01 M $Ag/AgNO_3$ electrode [in 0.1 M $(n\text{-Bu})_4NPF_6$−CH_3CN] was employed as the reference electrode, and a platinum electrode (Φ = 0.3 mm) was used as the supporting electrode. Redox potentials were reported versus the ferrocenium/ferrocene redox couple. Redox potential shifts were obtained after an excess of anions as their $(n\text{-Bu})_4N^+$ salts was added to the solution of receptors **4a** in CH_3CN (5.0×10^{-4} M) containing 0.1 M $(n\text{-Bu})_4NPF_6$.

CAChe 6.1.1 Program. A visual molecular model was computed using the *CAChe 6.1.1* program[23] to evaluate the shape of macrocycles **3**.

X-ray Structural Determinations. X-ray diffraction measurements were carried out at 291 K on a Bruker Smart Apex CCD area detector equipped with graphite-monochromated Mo Kα radiation

Table 2. Crystallographic Data for Complexes $1\cdot 2H_2O$, $1a\cdot 4H_2O$, and $4\cdot 2H_2O$

	$1\cdot 2H_2O$	$1a\cdot 4H_2O$	$4\cdot 2H_2O$
formula	$C_{56}H_{72}N_{16}O_{14}Pd_2$	$C_{56}H_{76}F_{24}N_{12}O_4P_4Pd_2$	$C_{48}H_{72}Fe_2N_{16}O_{14}Pd_2$
fw	1406.10	1773.97	1421.72
cryst size [mm]	0.20 × 0.22 × 0.28	0.22 × 0.24 × 0.28	0.22 × 0.24 × 0.28
cryst syst	monoclinic	monoclinic	triclinic
space group	$P2(1)/c$	$C2/c$	$P\bar{1}$
a [Å]	11.8736(18)	21.1271(10)	9.8461(6)
b [Å]	21.6334(15)	29.7501(15)	11.0730(7)
c [Å]	27.5290(16)	14.7561(8)	14.8140(9)
α [deg]	90.00	90.00	93.2950(10)
β [deg]	98.295(3)	103.105(1)	105.099(2)
γ [deg]	90.00	90.00	98.7650(10)
V [Å^3]	6997.3(12)	9033.2(8)	1533.13(16)
Z	4	4	1
ρ_{calcd} [g/cm^3]	1.335	1.304	1.540
μ [mm^{-1}]	0.582	0.560	1.113
$F(000)$	2896	3584	728
$2\theta_{max}$ [deg]	52.00	52.00	52.00
no. of unique data	13 730	8892	5991
no. of param	864	502	392
GOF [F^2][a]	1.06	1.00	1.06
R1 [$F^2 > 2\sigma(F^2)$], wR2 [F^2][b]	0.0546, 0.1236	0.0574, 0.1366	0.0489, 0.1035
$\Delta\rho_{max}$, $\Delta\rho_{min}$ [e/Å^3]	0.48, −0.81	0.75, −0.79	1.04, −0.57

[a] GOF = $[w(F_o^2 - F_c^2)^2]/(n-p)^{1/2}$, where n and p denote the number of data points and the number of parameters, respectively. [b] R1 = $(\sum||F_o| - |F_d||)/|F_o|$; wR2 = $[w(F_o^2 - F_c^2)^2]/[w(F_o^2)^2]^{1/2}$, where $w = 1/[\sigma^2(F_o^2) + (aP)^2 + bP]$ and $P = (F_o^2 + 2F_c^2)/3$.

(λ = 0.710 73 Å). The absorption correction for all complexes was performed using *SADABS*.[24] All of the structures were solved by direct methods, refined by employing full-matrix least squares on F^2 using the *SHELXTL* (Bruker, 2000) program, and expanded using Fourier techniques.[25] All non-H atoms of the complexes were refined with anisotropic thermal parameters. The H atoms were included in idealized positions. Final residuals along with unit cell, space group, data collection, and refinement parameters are presented in Table 2.

Synthesis. *{[(TMEDA)Pd]$_2$L$^1_2$}(NO$_3$)$_4$ (**1**).* (TMEDA)Pd(NO$_3$)$_2$ (41.6 mg, 0.12 mmol) was added to a suspension of L^1 (40.8 mg, 0.12 mmol) in H$_2$O (1 mL), and the mixture was stirred for 12 h at room temperature. The mixture was filtered, and the resulting clear yellow solution was evaporated to dryness to give a yellow solid. Pure **1**, as a microcrystalline light-yellow solid, was obtained by concentration of a methanol solution of **1**. Yield: 39.5 mg (48%). ^{1}H NMR (400 MHz, DMSO-d_6, 25 °C, Si(CH$_3$)$_4$, ppm): 8.19−8.16 (m, 8H), 7.58 (s, 4H), 7.54−7.51 (m, 8H), 7.51 (s, 4H), 7.45 (s, 4H), 6.25 (s, 8H, L^1−CH$_2$) 2.68 (s, 8H, TMEDA−CH$_2$), 2.15 (s, 24H, TMEDA−CH$_3$). ESI-MS (methanol, m/z): 1308.35 ([**1**−NO$_3^-$]$^+$), 623.2 ([**1**−2NO$_3^-$]$^{2+}$), 394.5 ([**1**−3NO$_3^-$]$^{3+}$), 280.6 ([**1**−4NO$_3^-$]$^{4+}$). Elem anal. Calcd for C$_{56}$H$_{68}$N$_{16}$Pd$_2$O$_{12}$·2H$_2$O: C, 47.83; H, 5.16; N, 15.94. Found: C, 47.79; H, 5.04; N, 15.66. X-ray-quality crystals were grown by the slow evaporation of a methanol solution of **1** at room temperature.

The PF$_6^-$ salt of **1** (**1a**) was prepared by exchange with a 10-fold excess of NH$_4$PF$_6$ in a methanol solution. ^{1}H NMR (400 MHz, DMSO-d_6, 25 °C, Si(CH$_3$)$_4$, ppm): 8.31−8.28 (dd, J_1 = 6.9 Hz, J_2 = 3.1 Hz, 8H), 8.14 (s, 4H), 7.52−7.49 (dd, J_1 = 6.9 Hz, J_2 = 3.1 Hz, 8H), 7.25 (s, 4H), 7.10 (s, 4H), 6.27 (s, 8H, L^1−CH$_2$) 2.86 (s, 8H, TMEDA−CH$_2$), 2.37 (s, 24H, TMEDA−CH$_3$). Elem anal. Calcd for C$_{56}$H$_{68}$N$_{12}$Pd$_2$P$_4$F$_{24}$·4H$_2$O: C, 37.91; H, 4.32; N, 9.47. Found: C, 37.79; H, 4.14; N, 9.36. X-ray-quality crystals were grown by the vapor diffusion of diethyl ether into a solution of **1a** in acetonitrile at room temperature.

*{[(TMEDA)Pt]$_2$L$^1_2$}(NO$_3$)$_4$ (**2**).* AgNO$_3$ (10.2 mg, 0.06 mmol) was added to a suspension of (TMEDA)PtCl$_2$ (11.5 mg, 0.03 mmol) in H$_2$O (1 mL), and the mixture was stirred at room temperature for 24 h in the dark. Then the mixture was filtered, to the colorless filtrate was added L^1 (10.2 mg, 0.03 mmol), and the system was stirred for 2 h at room temperature. After acetone (0.5 mL) was added, the system was heated at 60 °C for 24 h under stirring. After being filtered, the resulting clear yellow solution was evaporated to dryness to give a yellow solid. Pure **2**, as a light-yellow solid, was obtained by the vapor diffusion of diethyl ether into a solution of **2** in methanol at room temperature. Yield: 8.5 mg (37%). ^{1}H NMR (400 MHz, DMSO-d_6, 25 °C, Si(CH$_3$)$_4$, ppm): 8.14−8.12 (m, 8H,), 7.59 (s, 4H), 7.53−7.49 (m, 8H), 7.51 (s, 4H), 7.42 (s, 4H), 6.27 (s, 8H, L^1−CH$_2$) 2.72 (s, 8H, TMEDA−CH$_2$), 2.31 (s, 24H, TMEDA−CH$_3$). ESI-MS (methanol, m/z): 711.7 ([**2**−2NO$_3^-$]$^{2+}$), 324.8 ([**2**−4NO$_3^-$]$^{4+}$). Elem anal. Calcd for C$_{56}$H$_{68}$N$_{16}$Pt$_2$O$_{12}$·2H$_2$O: C, 42.48; H, 4.58; N, 14.15. Found: C, 42.26; H, 4.33; N, 13.83.

*{[(TMEDA)Pd]$_2$L$^2_2$}(NO$_3$)$_4$ (**3**).* (TMEDA)Pd(NO$_3$)$_2$ (10.4 mg, 0.03 mmol) was added to a suspension of L^2 (13.2 mg, 0.03 mmol) in H$_2$O (1 mL), and the mixture was stirred for 12 h at room temperature. After acetone (0.5 mL) was added, the system was heated at 60 °C for 24 h under stirring. The resulting clear yellow solution was evaporated to dryness to give a yellow solid. Pure **3**, as a yellow solid, was obtained by the vapor diffusion of diethyl ether into a solution of **3** in methanol at room temperature. Yield: 19.8 mg (84%). ^{1}H NMR (400 MHz, DMSO-d_6, 25 °C, Si(CH$_3$)$_4$, ppm): 9.09−9.07 (d, J = 8.2 Hz, 4H), 8.45−8.43 (dd, J_1 = 7.0 Hz, J_2 = 3.2 Hz, 4H), 8.21−8.19 (d, J = 8.2 Hz, 4H), 7.98 (s, 4H, C2−H), 7.87−7.85 (dd, J_1 = 7.0 Hz, J_2 = 3.2 Hz, 4H), 7.83−7.81 (dd, J_1 = 7.0 Hz, J_2 = 3.2 Hz, 4H), 7.80−7.76 (t, J = 7.8 Hz, 4H), 7.73−7.69 (t, J = 7.8 Hz, 4H), 7. 38−7.36 (dd, J_1 = 7.0 Hz, J_2 = 3.2 Hz, 4H), 6.66−6.63 (d, J = 14.5 Hz, 4H, L^2−CH$_2$), 6.38−6.34 (d, J = 14.5 Hz, 4H, L^2−CH$_2$), 2.96−2.90(b, 4H, TMEDA−CH$_2$), 2.74−2.67 (t, J = 13.3 Hz, 4H, TMEDA−CH$_2$), 2.49 (s, 12H, TMEDA−CH$_3$), 1.86 (s, 12H, TMEDA−CH$_3$). ESI-MS (methanol, m/z): 1508.4 ([**3**−NO$_3^-$]$^+$), 723.2 ([**3**−2NO$_3^-$]$^{2+}$), 461.5 ([**3**−3NO$_3^-$]$^{3+}$), 330.6 ([**3**−4NO$_3^-$]$^{4+}$). Elem anal. Calcd for C$_{72}$H$_{76}$N$_{16}$O$_{12}$Pd$_2$·2H$_2$O: C, 53.83; H, 5.02; N, 13.95. Found: C, 53.65; H, 4.91; N, 13.55.

*{[(TMEDA)Pd]$_2$L$^3_2$}(NO$_3$)$_4$ (**4**).* The same procedure as that employed for **1** was followed for the synthesis of **4**, except that L^3 (40.6 mg, 0.12 mmol) was used as the starting material. Yield: 71.2 mg (87%). ^{1}H NMR (400 MHz, CD$_3$CN, 25 °C, Si(CH$_3$)$_4$, ppm): 8.29 (s, 4H), 7.27 (s, 4H), 7.15 (s, 4H), 4.76 (s, 8H, L^3−CH$_2$), 3.98 (s, 8H), 3.70 (s, 8H), 2.92 (s, 8H, TMEDA−CH$_2$), 2.53 (s, 24H, TMEDA−CH$_3$). ESI-MS (methanol, m/z): 630.6 ([**4**−2NO$_3^-$]$^{2+}$), 399.7 ([**4**−3NO$_3^-$]$^{3+}$), 284.4 ([**4**−4NO$_3^-$]$^{4+}$). Elem anal. Calcd for C$_{48}$H$_{68}$Fe$_2$N$_{16}$Pd$_2$O$_{12}$·2H$_2$O: C, 40.55; H, 5.10; N, 15.76. Found: C, 40.59; H, 4.95; N, 15.58. X-ray-quality crystals were grown by the slow evaporation of a methanol solution of **4** at room temperature.

The PF$_6^-$ salt of **4** (**4a**) was prepared by exchange with a 10-fold excess of NH$_4$PF$_6$ in a methanol solution. ^{1}H NMR (400 MHz, CD$_3$CN, 25 °C, Si(CH$_3$)$_4$, ppm): 8.03 (s, 4H), 7.25 (s, 4H), 7.16 (s, 4H), 4.76 (s, 8H, L^3−CH$_2$), 3.97 (s, 8H), 3.67 (s, 8H), 2.93 (s, 8H, TMEDA−CH$_2$), 2.55 (s, 24H, TMEDA−CH$_3$). Elem anal. Calcd for C$_{48}$H$_{68}$Fe$_2$N$_{12}$P$_4$F$_{24}$Pd$_2$·2H$_2$O: C, 32.88; H, 4.14; N, 9.59. Found: C, 32.76; H, 4.05; N, 9.38.

*{[(TMEDA)Pt]$_2$L$^3_2$}(NO$_3$)$_4$ (**5**).* The same procedure as that employed for **2** was followed for the synthesis of **5**, except that L^3 (10.4 mg, 0.03 mmol) was used as the starting material. Yield: 7.9 mg (33%). ^{1}H NMR (400 MHz, MeOD, 25 °C, ppm): 8.61 (s, 4H), 7.37−7.37 (d, J = 1.1 Hz, 8H), 4.97 (s, 8H, L^3−CH$_2$), 4.16−4.15 (t, J = 1.8 Hz, 8H), 3.85−3.84 (t, J = 1.7 Hz, 8H), 3.07 (s, 8H, TMEDA−CH$_2$), 2.78 (s, 24H, TMEDA−CH$_3$). ESI-MS (methanol, m/z): 1501.3 ([**5**−NO$_3^-$]$^+$), 719.7 ([**5**−2NO$_3^-$]$^{2+}$), 459.1 ([**5**−3NO$_3^-$]$^{3+}$), 328.8 ([**5**−4NO$_3^-$]$^{4+}$). Elem anal. Calcd for C$_{48}$H$_{68}$Fe$_2$N$_{16}$Pt$_2$O$_{12}$·2H$_2$O: C, 36.05; H, 4.54; N, 14.02. Found: C, 35.74; H, 4.37; N, 13.88.

■ ASSOCIATED CONTENT

Supporting Information. ^{1}H NMR spectra of **1**, **1a**, **2**−**4**, **4a**, and **5**, ESI-MS spectra of **2**−**5**, packing diagrams of **1**, **1a**, and **4**, tables of selected bond lengths and angles for **1**, **1a**, and **4**, fluorescence spectra, CV spectra, and X-ray crystallographic files for complexes **1**, **1a**, and **4** in CIF format. This material is available free of charge via the Internet at http://pubs.acs.org.

■ AUTHOR INFORMATION

Corresponding Author
*E-mail: yusy@ruc.edu.cn.

■ ACKNOWLEDGMENT

This project was supported by the National Natural Science Foundation of China (Grant 51073171), the Beijing Natural Science Foundation (Grant 2112018), and the Graduate Science Research Foundation of Renmin University of China (Grant 22396155).

■ REFERENCES

(1) Lehn, J.-M. *Supramolecular Chemistry: Concepts and Perspectives*; VCH: Weinheim, Germany, 1995.

(2) Bianchi, A., Bowman-James, K., García-España, E., Eds. *Supramolecular Chemistry of Anions*; Wiley-VCH: New York, 1997.

(3) Mingos, D. M. P.; Ramón, V. *Structure and Bonding, Recognition of Anions*; Springer-Verlag: Berlin, 2008.

(4) (a) Gale, P. A. *Coord. Chem. Rev.* **2000**, *199*, 181–233. (b) Gale, P. A. *Coord. Chem. Rev.* **2001**, *213*, 79–128. (c) Beer, P. D.; Gale, P. A.

Angew. Chem., Int. Ed. **2001**, *40*, 487–516. (d) Gale, P. A. *Chem. Soc. Rev.* **2010**, *39*, 3746–3771.

(5) (a) Bowman-James, K. *Acc. Chem. Res.* **2005**, *38*, 671–678. (b) Kang, S. O.; Llinares, J. M.; Day, V. W.; Bowman-James, K. *Chem. Soc. Rev.* **2010**, *39*, 3980–4003.

(6) (a) Amendola, V.; Fabbrizzi, L.; Mosca, L. *Chem. Soc. Rev.* **2010**, *39*, 3889–3915. (b) Duke, R. M.; Veale, E. B.; Pfeffer, F. M.; Kruger, P. E.; Gunnlaugsson, T. *Chem. Soc. Rev.* **2010**, *39*, 3936–3953. (c) Li, A.-F.; Wang, J.-H.; Wang, F.; Jiang, Y.-B. *Chem. Soc. Rev.* **2010**, *39*, 3729–3745.

(7) Snowden, T. S.; Anslyn, E. V. *Curr. Opin. Chem. Biol.* **1999**, *3*, 740–746.

(8) Martínez-Máñez, R.; Sancenón, F. *Chem. Rev.* **2003**, *103*, 4419–4476.

(9) (a) Wong, W. W. H.; Vickers, M. S.; Cowley, A. R.; Paul, R. L.; Beer, P. D. *Org. Biomol. Chem.* **2005**, *3*, 4201. (b) Chellappan, K.; Singh, N. J.; Hwang, I.-C.; Lee, J. W.; Kim, K. S. *Angew. Chem., Int. Ed.* **2005**, *44*, 2899–2903.

(10) (a) Seidel, S. R.; Stang, P. J. *Acc. Chem. Res.* **2002**, *35*, 972–983. (b) Würthner, F.; You, C.-C.; Saha-Möller, C. R. *Chem. Soc. Rev.* **2004**, *33*, 133–146. (c) Fujita, M.; Tominaga, M.; Hori, A.; Therrien, B. *Acc. Chem. Res.* **2005**, *38*, 371–380. (d) Yu, S.-Y.; Li, S.-H.; Huang, H.-P.; Zhang, Z.-X.; Jiao, Q.; Shen, H.; Hu, X.-X.; Huang, H. *Curr. Org. Chem.* **2005**, *9*, 555–563.

(11) (a) Bondy, C. R.; Gale, P. A.; Loeb, S. J. *J. Am. Chem. Soc.* **2004**, *126*, 5030–5031. (b) Vega, I. E. D.; Gale, P. A.; Light, M. E.; Loeb, S. J. *Chem. Commun.* **2005**, 4913–4915.

(12) (a) Yu, S.-Y.; Huang, H.; Liu, H.-B.; Chen, Z.-N.; Zhang, R.; Fujita, M. *Angew. Chem., Int. Ed.* **2003**, *42*, 686–690. (b) Yu, S.-Y.; Huang, H.-P.; Li, S.-H.; Jiao, Q.; Li, Y.-Z.; Wu, B.; Sei, Y.; Yamguchi, K.; Pan, Y. J.; Ma, H.-W. *Inorg. Chem.* **2005**, *44*, 9471–9488. (c) Li, S.-H.; Huang, H.-P.; Yu, S.-Y.; Li, Y.-Z.; Huang, H.; Sei, Y.; Yamaguchi, K. *Dalton Trans.* **2005**, 2346–2348. (d) Huang, H.-P.; Li, S.-H.; Yu, S.-Y.; Li, Y.-Z.; Jiao, Q.; Pan, Y.-J. *Inorg. Chem. Commun.* **2005**, *8*, 656–660. (e) Liu, L.-X.; Huang, H.-P.; Li, X.; Sun, Q.-F.; Sun, C.-R.; Li, Y.-Z.; Yu, S.-Y. *Dalton Trans.* **2008**, *12*, 1544–1546. (f) Li, X.; Li, H.; Yu, S.-Y.; Li, Y.-Z. *Sci. China, Ser. B: Chem.* **2009**, *52*, 471–474. (g) Ning, G.-H.; Xie, T.-Z.; Pan, Y.-J.; Li, Y.-Z.; Yu, S.-Y. *Dalton Trans.* **2010**, *39*, 3203–3211. (h) Ning, G.-H.; Yao, L.-Y.; Liu, L.-X.; Xie, T.-Z.; Li, Y.-Z.; Qin, Y.; Pan, Y.-J.; Yu, S.-Y. *Inorg. Chem.* **2010**, *49*, 7783–7792.

(13) Kaplan, L.; Kester., W. L.; Katz, J. J. *J. Am. Chem. Soc.* **1952**, *74*, 5531–5532.

(14) (a) Smit, K. J.; Ghiggino, K. P. *Chem. Phys. Lett.* **1985**, *13*, 369. (b) Xie, H.; Yi, S.; Yang, X.; Wu, S. *New J. Chem.* **1999**, *23*, 1105–1110.

(15) Fery-Forgues, S.; Delavaux-Nicot, B. *J. Photochem. Photobiol., A* **2000**, *132*, 137.

(16) Otón, F.; Tárraga, A.; Espinosa, A.; Velasco, M. D.; Molina, P. *J. Org. Chem.* **2006**, *71*, 4590.

(17) (a) Thomas, J.-L.; Howarth, J.; Hanlon, K.; Mcguirk, D. *Tetrahedron Lett.* **2000**, *41*, 413–416. (b) Thomas, J.-L.; Howarth, J.; Kennedy, A. M. *Molecules* **2002**, *7*, 861–866.

(18) Armarego, W. L. F.; Perrin, D. D. *Purification of Laboratory Chemicals*; 4th ed.; Butterworth Heinemann: Oxford, U.K., 1997.

(19) Willermann, M.; Mulcahy, C.; Lippert, B. *Inorg. Chem.* **2006**, *45*, 2093.

(20) Neelakandan, P. P.; Ramaiah, D. *Angew. Chem., Int. Ed.* **2008**, *47*, 8407–8411.

(21) Du, J.-L.; Hu, T.-L.; Zhang, S.-M.; Zeng, Y.-F.; Bu, X.-H. *CrystEngComm* **2008**, *10*, 1866–1874.

(22) Niu, H.-T.; Yin, Z.-M.; Su, D.-D.; Niu, D.; He, J.-Q.; Cheng, J.-P. *Dalton Trans.* **2008**, 3694–3700.

(23) *CACh*e *6.1.1 for Windows*; Fujitsu Ltd.: Chiba, Japan, 2003.

(24) Sheldrick, G. M. *SADABS, Program for area detector adsorption correction*; Institute for Inorganic Chemistry, University of Göttingen, Göttingen, Germany, 1996.

(25) Sheldrick, G. M. *SHELXTL NT, Program for Solution and Refinement of Crystal Structures*, version 5.1; University of Göttingen: Göttingen, Germany, 1997.